Version of Record: https://www.sciencedirect.com/science/article/pii/S0927775721008190
Manuscript_4ea920189792e050a3380dceee5e03db

Biocompatible and biomimetic keratin capped Au nanoparticles enable the inactivation of mesophilic bacteria via photo-thermal therapy☆

Ferdinanda Annesi[a,*], Alfredo Pane[a,*], Luigia Pezzi[a,1,*], Pasquale Pagliusi[a,c], Maria Adele Losso[b], Barbara Stamile[b], Antonio Qualtieri[d], Giovanni Desiderio[a], Marco Contardi[e], Athanassia Athanassiou[e], Giovanni Perotto[e,1], Luciano De Sio[f,a,1]

[a] *CNR-Lab. Licryl, Institute NANOTEC, 87036 Arcavacata di Rende, Italy.*
[b] *Department DiBEST (Biology, Ecology and Earth Sciences), University of Calabria, 87036 Arcavacata di Rende, Italy.*
[c] *Department of Physics, University of Calabria, 87036, Arcavacata di Rende, Italy.*
[d] *CNR Institute for Biomedical Research and Innovation, IRIB. Piano Lago, 87050 Mangone (CS), Italy.*
[e] *Smart Materials,, Istituto Italiano di Tecnologia (IIT), Via Morego 30, 16163 Genoa, Italy.*
[f] *Department of Medico-Surgical Sciences and Biotechnologies, Center for Biophotonics, Sapienza University of Rome, Corso della Repubblica 79, 04100 Latina, Italy*

Abstract

We report on the synthesis, characterization, and application of biomimetic, spherical Au nanoparticles (AuNPs) coated with keratin (Ker-AuNPs). They are characterized in terms of morphological, spectral, and thermo-optical properties. Besides their excellent colloidal stability, Ker-AuNPs exhibit excellent biocompatibility. The latter is verified by performing viability assay experiments of a strain of *Escherichia coli* (*E. coli*) in the presence of Ker-AuNPs as a function of the incubation time. Ker-AuNPs do not affect the *E. coli* viability and proliferation, even at the highest concentration tested (C=$5.83 * 10^{-5}$ M). Photo-thermal assisted viability experiments are performed by setting the starting temperature at 37 ^{o}C, mimicking the normal human body temperature condition. They evidence the capability of the Ker-AuNPs to generate a temperature up to about 73 ^{o}C (an increase of 36 ^{o}C), thus reducing the viability of

☆ Article contains supplementary informations
* Authors contibuted equally
[1] Corresponding authors: luigia.pezzi@cnr.it (Luigia Pezzi); giovanni.perotto@iit.it (Giovanni Perotto); luciano.desio@uniroma1.it (Luciano De Sio)

© 2021 published by Elsevier. This manuscript is made available under the Elsevier user license
https://www.elsevier.com/open-access/userlicense/1.0/

bacterial cells 3 order of magnitudes. We also conducted a theoretical analysis with an ad-hoc model that evidences an excellent agreement between theory and experiments. Ker-AuNPs represent a new generation of multifunctional nanotherapeutics, and they constitute a new opportunity in drug-free and minimally invasive biomedical applications.

1. Introduction

Gold nanoparticles (AuNPs) have been largely explored in the past few decades for their intrinsic chemical, optical and size-dependent properties. Specifically, the ability of AuNPs to convert a monochromatic (resonant) light into thermal energy (photo-thermal effect) has marked their utilization in cancer and other pathogenic disease treatments through the so-called photo-thermal therapy (PTT)[1, 2, 3, 4]. AuNPs-mediated PTT exploits the efficient conversion of light into heat produced by the strong absorption associated with a physical phenomenon called localized plasmonic resonance (LPR)[5]. Indeed, under a suitable light illumination, AuNPs exhibit a coherent and dipolar oscillation of the bulk-free electrons localized at the metallic/dielectric interface. As a consequence, because of the strong absorption associated with the LPR mechanism, there is a noticeable temperature increase, thus turning the AuNP into an excellent hot-spot to be used for PTT-based medical applications[6]. A pharmaceutical formulation for PTT treatments based on the utilization of AuNPs requires the following properties: water-dispersion, chemical stability, photothermal efficiency, and biocompatibility. The latter can be drastically compromised if the capping (dielectric) material utilized to stabilize the AuNPs induces toxicity effects[7]. The most common and reliable technique utilized for the synthesis of AuNPs is based on the Turkevich method[8], a chemical route that allows the synthesis of water dispersable AuNPs with a small size distribution, high uniformity, and reproducibility. One of the Turkevich method's main drawbacks is the utilization of citrate as a capping agent, which, in turn, provides low colloidal stability that results in the irreversible AuNPs aggregation

in the physiological environment. To address this issue, and to be able to engineer the shape into rods, stars and pyramids, commercially available AuNPs are stabilized through cationic surfactants (e.g., cetyltrimethylammonium bromide, CTABs), which unfortunately, exhibit very high intrinsic toxicity[9, 10], limiting their use for bio-related applications. Bio-polymer based capping agents have received considerable attention in the past years because they can provide high colloidal stability, biocompatibility, and biomimicry[11]. Biomaterials and proteins are unique materials for realizing innovative and functionalized AuNPs with better biocompatibility, biodistribution, stability, and half-life. Keratins - a group of cysteine-rich fibrous proteins found in hairs, nails, and horns - are a class of attractive materials due to their biocompatibility and renewable origins. Besides, keratin proteins own amino acid sequences that are very similar to those present on the extracellular matrix (ECM), thus representing a source for the design of biomaterials that can be readily accepted by the human body and promote cellular attachment, proliferation, and migration [12]. Recently, keratins have also been used for the production of keratin-based NPs and applied in various biomedical[13, 14, 12] and recently also technological areas [15]. For instance, Zhang et al. [16] reported a new antibacterial strategy by realizing Silver NPs (AgNPs) from super-heated water degraded keratin solutions. In a different approach, Tran et al. have shown that both AgNPs[17] and AuNPs[18] combined with composites made of cellulose and keratin possess high biocompatibility and strong antimicrobial activity. Skankar et al. [19] have recently realized a new generation of eco-friendly antimicrobial NPs by adsorbing metal ions to keratin NPs. More recently, we have reported on the synthesis and application of an innovative biocompatible, and biomimetic spherical NPs made of Au surrounded by a thin layer of keratin (Ker-Au NPs) [20]. The biomimetic property of Ker-Au NPs is associated with the combination of a synthetic material (Au) and a natural material (keratin). Herein, we report a novel PTT-based medical application by exploiting the outstanding properties of Ker-Au NPs. Ker-Au NPs were characterized by morphological, spectroscopic, fluorescence microscopy, Fourier Transform Infrared Spectroscopy

(FTIR), and infrared thermography. Biocompatibility experiments, PTT-based treatments, and viability assays were performed by utilizing *Escherichia coli* (*E. coli)*, a gram-negative and mesophilic bacteria. Results evidenced that Ker-AuNPs represent a advanced biocompatible NPs with outstanding optical and thermo-optical properties, thus opening a new road towards the realization of innovative, PTT-based, high-precision medical treatments.

2. Material and methods

Keratin Extraction. Keratin proteins were extracted from wool fibers with a protocol reported in [22] Wool fibers, obtained from a textile company, were degreased using a 1:1 methanol/acetone solution. The degreasing step was performed by agitation at room temperature, and fibers were washed twice with clean solvents. Fibers were then washed twice with Milli-Q water and allowed to dry at room temperature for 24 hours. Keratin was extracted from the cleaned wool fibers using a 7 M water solution of urea with the aid of 0.05 M sodium dodecyl sulfate (SDS) and 1.1 M 2-mercaptoethanol. The extraction was performed at 60 ^{o}C for 5 hours using 18 mL of solution for each fiber gram. After the extraction, the solution was filtered with a 50-mesh stainless steel grid to remove undissolved fibers and then dialyzed against Milli-Q distilled water for three days with seven water changes. The dialyzed solution had a keratin concentration of around 15 mg/mL and was purified from residual fibers and debris by centrifugation. The concentration of proteins was measured by drying a known volume of the dialyzed solution.

Synthesis of Ker-AuNPs. The synthesis of Ker-AuNPs was performed in two stages: at first spherical AuNPs were synthesized using the procedure developed by Turkevich [8] using sodium citrate. After the synthesis, the 1.5 mM Au solution was mixed with the keratin solution to allow the keratin proteins to bind to the AuNPs. The mass ratio between keratin and Au was 100 to 1. After letting the keratin and Au to rest overnight, the NPs were purified to remove

non-bounded keratin proteins. This step was performed by centrifugation at 16128 g and resuspension in MilliQ water twice.

Fluorescently labelled Ker-AuNPs. To realize fluorescently labeled Ker-AuNPs (Ker*-AuNPs), keratin was first labeled by using the FluoReporter FITC Protein Labeling Kit (ThermoFisher, Whaltam, MA). A buffer solution of NaHCO3 1 M, pH 9, was prepared. 1955 μL of buffer and 45 μL of keratin solution 44 mg/mL were mixed to obtain 2 mL of solution with a final keratin concentration of 1 mg/mL. FITC powder was dissolved in 10 μL of DMSO. The solubilized FITC was added to the buffered keratin solution and mixed under stirrer for 1 hour in dark condition at room temperature. The keratin-FITC solution was dialyzed in a dialysis cassette with a molecular weight cut off (MWCO) of 3500 kDa for three days against MilliQ water. Ker*-AuNPs were synthesized using the same protocol used for Ker-AuNPs.

UV-Vis and Infrared spectroscopy. UV-Vis absorption spectra were acquired with a UV-Vis light source (CLS 100, Leica) equipped with a spectrometer (USB 2000+XR1, Ocean Optics). Fourier Transformed Infrared Spectroscopy (FTIR) was performed with a Vertex spectrometer in transmission mode using KBr pellets. Keratin and Ker-AuNPs were cast from their respective water solutions on 150 mg of KBr and allowed to dry for 48 hours at 50 ^{o}C. Samples were then finely ground with a mortar and pressed into a pellet. The baseline was acquired using a blank KBr pellet. Spectra were measured from 400 cm^{-1} to 4000 cm^{-1} with a resolution of 4 cm^{-1} and the acquisition of 64 scans.

Transmission electron microscopy imaging. Transmission electron microscopy (TEM) images were recorded on a JEOL JEM-1011 operating at 100 kV. One drop of Ker-AuNP solution was cast on a TEM grid (100 mesh Cu grid coated with an ultrathin carbon) that was previously plasma treated to increase hydrophilicity. Excess solution was wicked off from the grid's side, and then the grid was allowed to dry for at least 24 hours before imaging.

Fluorescence microscopy analysis. Fluorescence microscopy analysis was carried out using a conventional fluorescence microscope (Nikon Microphot-FX, Japan) equipped with phase contrast objectives and a Canon EOS 1300D camera. The specimen's green fluorescence was detected by using excitation light at 488nm and a 520 nm emission filter. The specimen was observed by oil immersion high magnification (100X) objective.

Growth curves of *E. coli* TG1 with and without Ker-AuNPs solutions. A gram-negative bacterial strains *E. coli* TG1, kindly provided by Prof. Michele Galluccio (University of Calabria), were culture in sterile Luria-Bertani (LB) broth (NaCl 5 g/L; yeast extract 5 g/L; trypton10 g/L) in aerobiosis at 37^{o}C over-night under shaking. 400 μL of over-night culture was diluted in 20 mL (1:50) of fresh LB broth to restart the cell cycle, incubated to 37^{o}C until the optical density at 600 nm (OD_{600}) reached the value of 0.4-0.6. At this OD value, the growth rate is constant, and the cells are already dividing and result in being metabolically active. Ker-AuNPs 424 μL was added in *E. coli* culture so that the total volume was 8 mL and the final concentration of Ker-AuNPs was about $5.83 * 10^{-5}$ M. The OD_{600} values of the samples were recorded after 1, 3, 6, 24 hours of incubation at 37 ^{o}C to monitor the growth curve of the bacteria with and without Ker-AuNPs. At any incubation time, serial dilutions (from 10^{-1} to 10^{-6}) of both cultures in LB broth were made, and 50 μL of each dilution was spread onto sterile LB agar (LB broth with agar 16 g/L) and incubated at 37 ^{o}C for 16-18 h. The log N cells were calculated by counting the Colony Forming Unit (CFU) and using the formula: CFU/mL =(N^o of colonies x dilution factor)/volume of the culture spread.

Thermal effect of *E. coli* TG1/Ker-AuNPs solutions. To verify the temperature effect on the cell viability, thermal experiments of *E. coli* with Ker-AuNPs solution were performed. 500 μL of *E. coli* culture (10^7 CFU/mL) with and without 26.5 μL of Ker-AuNPs solution ($5.83*10^{-5}$ M) was deposited in the sterile Eppendorf tube. Using a thermoblock instrument, the temperature was increased every 5 minutes from 54 ^{o}C until 78 ^{o}C and measured by a thermal-

camera. A series of dilutions from 10^{-1} to 10^{-5} in LB broth were made at any selected temperature, and 50 μL of each diluted sample was spread onto sterile LB agar and incubated at 37 ^{o}C over-night.

Photothermal characterization of *E. coli* TG1/ Ker-AuNPs solutions. The solution of *E. coli* bacteria is prepared as previously described: 211 μL of bacteria solution, and 11.2 μL of Ker-AuNPs solution with concentration $5.83 * 10^{-5}$ M were placed in a sterile Eppendorf (volume 0.2 mL). The latter was placed in a polystyrene box, enclosed in a heating box and thermostated at the body temperature T_i (Figure 1a). The polystyrene box (with low thermal conductivity 0.035 Wm^{-1} K^{-1}) minimizes the heat exchange between the sample and the environment to approximate an isolated system. The Eppendorf was illuminated from the top by a CW green laser beam (Ventus 532, Laser Quantum) with diameter $\sim$ 1.5 mm, TEM_{00} spatial mode profile, power P = 200 mW, wavelength $\lambda = 532$ nm. The induced resonant photo-thermal heating is acquired through a thermal-camera ('thermal imager' in Figure 1a) placed on the top of the sample. Figure 1b shows a sketch of the sample surface illuminated by the green laser The FLIR®E40 thermal-camera (FLIR®Systems, Inc.) acquires the sample's IR-emission and convert it into a color map (see Figure 1c: yellow represents the highest achieved temperature and red the starting temperature). Figure 1d shows a temperature plot obtained as a cut along the white line diameter (Figure 1c).

Morphological characterization *E. coli* TG1/ Ker-AuNPs solutions. SEM (scanning electron microscope) images were acquired using a quanta FEG 400 (FEI) in high vacuum mode and using an ETD (Everhart-Thornley Detector) sensor type were prepared by dehydrating both *E. coli* and *E. coli*/Ker-AuNPs solutions on glass chips, using 70%, 80%, 90%, 95%, and 100% ethanol, respectively, for 10 minutes steps. Subsequently, samples were fixed using a 3% glutaraldehyde in PBS, pH 7.3 solution, and left to dry overnight. Bacterial suspension treated with fluorescein linked Ker*-AuNPs (C=$5.83 * 10^{-5}$ M) for 1 h a 37 ^{o}C was centrifuged for 3 minutes at 1792 g, and the pellet washed three

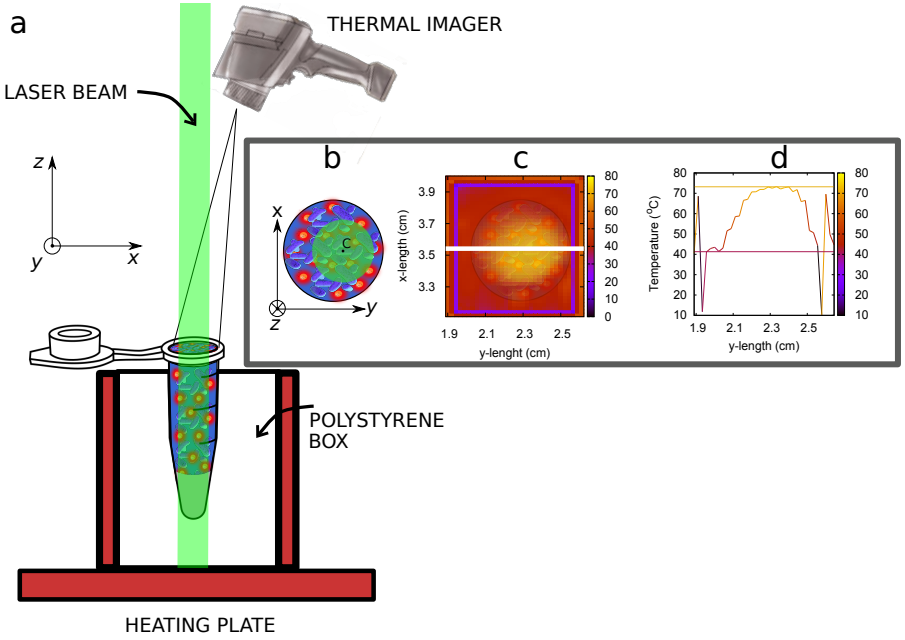

Figure 1: (a) Schematic representation of the optical setup and (b) of the sample surface with the waist of the green laser impinging on the solution. (c) Thermal image of the sample during the PTT experiment overlapped with panel (b) for reference. (d) A plot of temperature measured on the sample along the white section shown in panel (c). The point C in panel (b) represents the point in which the temperature is calculated in paragraph 4.

times with PBS. The pellet was re-suspended in PBS (200 μL), and 20 μL were laid onto a microscope glass slide, mounted with a coverslip, and sealed at the border by nail polish. The specimen was observed under a conventional fluorescence microscope (Nikon Microphot-FX, Japan) using a 488 nm excitation light and a 520 nm filter to detect the green emitted light. Phase contrast objectives also observed the same microscopic field. The microscopic images were acquired using a Canon EOS1300D camera, and the micrographs were processed using ImageJ software.

3. Experimental Results

Figure 2a shows the absorption spectrum of Ker-AuNPs dispersed in water with a typical LPR band centered at 534 nm. TEM image (Figure 2b) highlights both spherical geometry and the homogeneous size distribution of the Ker-AuNPs population. FTIR characterization is reported in Figure 2c. Ker-AuNPs spectrum (blue curve) shows the presence of the main peaks associated with keratin: the Amide I C=O stretching at 1600-1650 cm^{-1}, the Amide II N-H bending at 1450 cm^{-1}, and the Amide III absorption at 1235 cm^{-1}, moreover, the sample shows also the Amide A stretching at 3300 cm^{-1}, another fingerprint of the presence of protein on the surface. All these absorption bands are also present in the control spectrum of pure keratin (red curve). The absorption band between 1615 cm^{-1} and 1650 cm^{-1} in the spectra of AuNPs (black curve) is associated with the citrate ions bound on the surface of AuNPs. [21].

To test the effect of Ker-AuNPs (C=$5.83 * 10^{-5}$ M) solution on the *E. coli* TG1 growth, viability assay experiments at 1, 3, 6 and 24 h incubation time were performed. Figure 3 shows bacteria's viability with (green curve) and without (blue curve) Ker-AuNPs at 37^{o}C. Data demonstrates that Ker-AuNPs do not exhibit inhibitory effects on the bacteria growth as compared to *E. coli* growth without Ker-AuNPs. The two growth curves trend is similar (Figure 3), and bacteria growth turns out to be regular. Thermal experiments to verify the effect of the temperature on bacteria's viability were performed using a thermoblock.

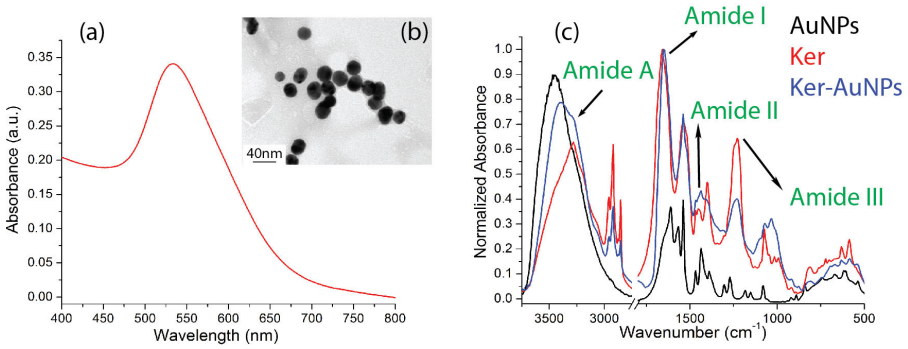

Figure 2: UV-Vis absorption spectrum (a) of Ker-AuNPs dispersed in water along with a representative TEM image (b). FTIR spectra (c) of pristine AuNPs (black), Keratin (red) and Ker-AuNPs (blue).

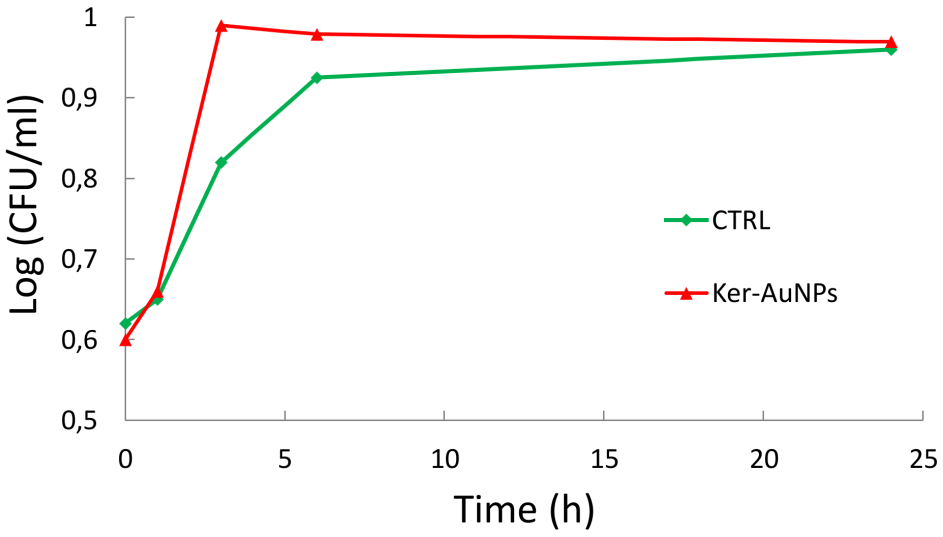

Figure 3: Cellular viability experiments at different incubation times (37 ^{o}C) without and with Ker-AuNPs solution (C=$5.83 * 10^{-5}$ M).

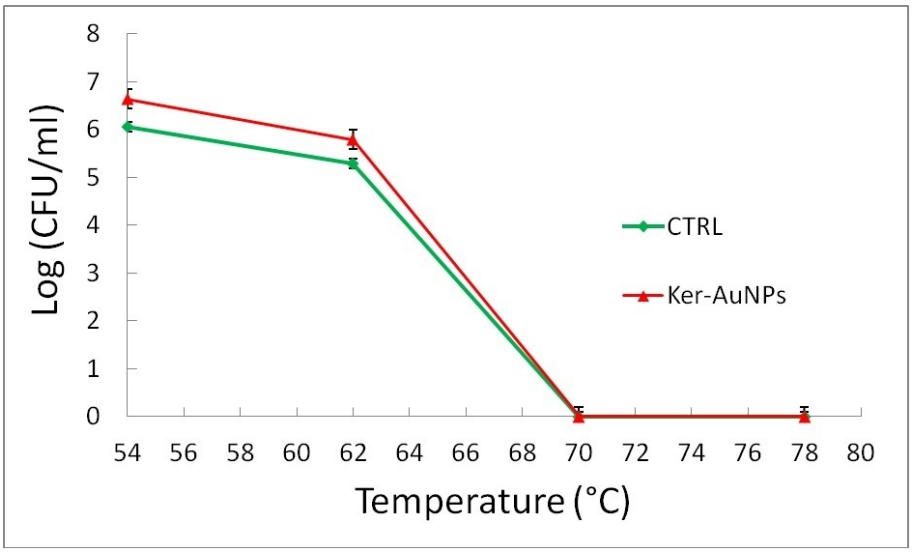

Figure 4: Cellular viability test without and with Ker-AuNPs(C=$5.83 * 10^{-5}$ M) at different temperatures. The grey bar shows the bacterial concentration not subject to heating.

500 μL of $\sim 10^7$ CFU/ml *E. coli* was heated from 54 ^{o}C to 78 ^{o}C for 5 minutes of incubation bacteria's viability is shown in (Figure 4). After 60 ^{o}C, a decrease of the CFU/ml was observed, eventually bacteria death occurred in the range 62 ^{o}C<T$\leq$70 ^{o}C . The thermal effect on bacteria suspension in the presence of $5.83 * 10^{-5}$ M Ker-AuNPs solution shows the same reduction in viability, and the two curves (Figure 4, red and green) do not significantly differ.

Fluorescence Microscopy and Scanning Electron Microscopy measurements. To verify possible specific interactions and uptake capability of Ker-AuNPs toward bacterial cells, a culture of *E. coli* TG1 was treated with Ker*-AuNPs. The optical images were taken in phase contrast and fluorescence microscopy (Figure 5), confirming that Ker*-AuNPs are uniformly distributed in the medium without evidence of significant aggregation, confirming the superior stability granted by the keratin coating. Also no signs of aggregated AuNP on bacterial cells were seen. Moreover, the images show that there is no evidence of intra-cellular fluorescent material accumulation. ESEM images

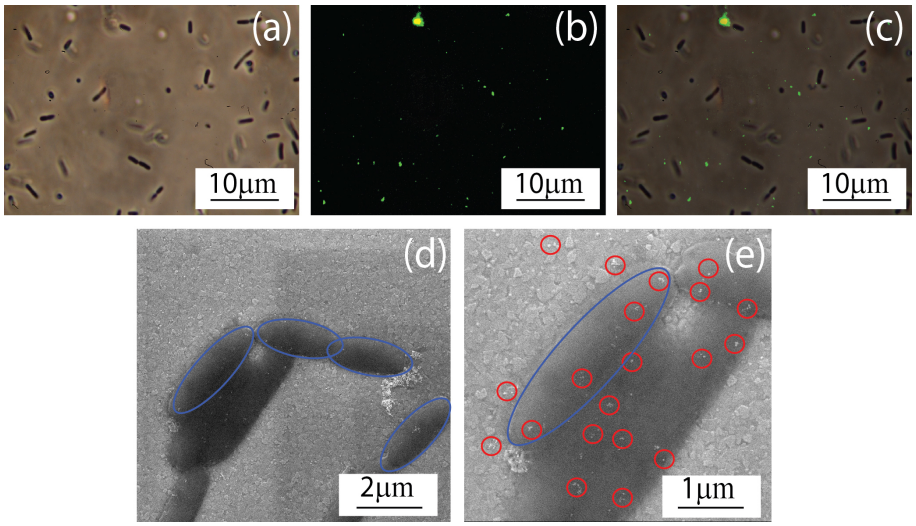

Figure 5: Microscopic analysis of*E. coli* TG1 incubated with Ker*-AuNPs. Phase-contrast microscopy at 100x magnification (a) along with the same view analyzed under green fluorescence (b), while (c) is the merged image. ESEM images of *E. coli* TG1 incubated with Ker-AuNPs at different magnification levels (d, e). The blue lines highlight the *E. coli* TG1 morphology while the red circles the presence of Ker-AuNPs.

(Figure 5 d, e) show the morphology of *E. coli* TG1 in the presence of Ker-AuNPs deposited on an ITO-coated glass substrate. The ITO layer's presence allows obtaining a perfect contrast between the organic (*E. coli* TG1) and inorganic (Ker-AuNPs) components without any evident damage associated with the high-energy electron beam. Results (Figure 5 d, e) confirm the absence of significant intra-cellular material accumulation and show a well-preserved bacteria morphology. Therefore, these observations suggest that Ker-AuNPs do not exhibit a specific interaction with the bacterial cells since they are visible on both the substrate and the bacteria's surface.

Photo-thermal results. Figure 6 shows the viability of *E. coli* TG1 before and after the photo-thermal experiments. In detail, the blue histogram reports the Log base 10 of the colonies forming units per milliliter in the *E. coli* TG1 solution ($Log_{10}\frac{CFU}{ml}$) prepared according to the protocol reported in the material and method section. The light blue histogram highlights a moderate change

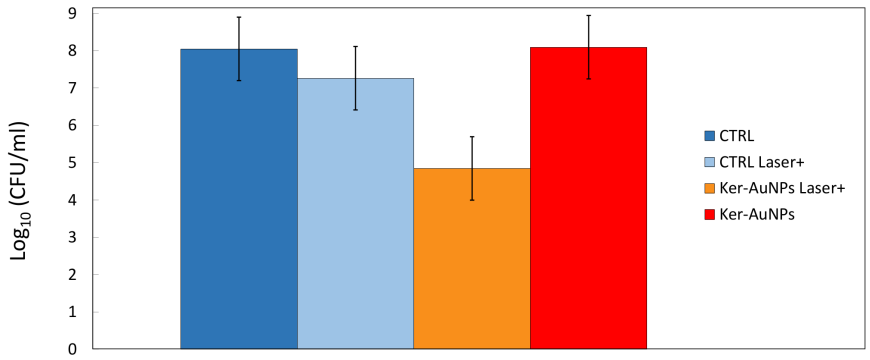

Figure 6: Results of the cellular viability assays carried out without and with Ker-AuNPs (C= $5.83 * 10^{-5}$ M) after 5 minutes of laser illumination

(less than 1 order of magnitude) of the *E. coli* TG1 viability after 5 minutes of laser illumination without Ker-AuNP. This behavior is attributed due to the intrinsic absorption of *E. coli* TG1 at 532 nm. The yellow histogram reports a significant reduction of *E. coli* TG1 viability in the presence of Ker-AuNPs under laser illumination. The light induced temperature change due to the photo-thermal conversion properties of Ker-AuNPs produces a temperature increase of about 36 ^{o}C (73 ^{o}C is the highest temperature), thus producing a reduction of *E. coli* TG1 of about 3 order of magnitudes. The red histogram is a control experiment performed by keeping the sample (*E. coli* TG1/Ker-AuNPs) at 37 ^{o}C for 5 minutes without laser illumination. This result confirms the exceptional stability and high compatibility of Ker-AuNPs, even in the presence of *E. coli* TG1 at 37 ^{o}C. It's worth pointing out that the initial cell viability, expressed in Log (CFU/ml), reported in the experiments performed in Figures 4 and 6, are different. This difference is attributed to the utilization of different *E. coli* cultures. However, it is important to stress out that the cells were in the log phase of the growth curve in both cases.

4. Theoretical prediction

When a light beam of suitable wavelength impinges on a metal NP (MNP), its conductive band's electrons start to oscillate coherently with the impinging light's electric field. This phenomenon results in a strong absorption responsible for a localized heat production [23, 24, 25]. In this framework, AuNPs have gained an important role because their LPR can be tuned from the visible to the near-infrared (NIR) range by simply changing size, shape, or dielectric function of the surrounding medium [26, 27, 28, 29, 30]. Moreover, AuNPs are biocompatible and can be easily functionalized with a large variety of molecules, exhibiting also a weak oxidation. Thanks to these properties, AuNPs have been widely exploited in cancer therapy [31, 32, 33, 34, 35], ophthalmology and dermatology, nanosurgery [36, 37], photothermal drug delivery and gene therapy [38, 39, 40], photothermal imaging [41], plasmon-assisted nanochemistry [42], plasmon-assisted optofluidics [43] and sensing [44, 45]. Each NP becomes a nano-source of heat that produce nano-localized temperature variation [26, 27, 46, 47] but its collective effect is able to produce also a macroscopic temperature variation depending on the number of illuminated NPs [46, 48]. In our experiments we observe a global macroscopic temperature variation (Figure 1c, d). Our theoretical goal is to calculate and predict the macroscopic temperature variation, in the center C of laser spot size (see point C in the inset Figure 1b), due to the collective effect of spherical AuNPs participating in the solution. Assuming that only the illuminated NPs contribute to the global temperature (cylindrical symmetry) and taking into account the attenuation of light (Lambert-Beer law) we are able to obtain the formula 1 that provides the temperature variation in the C point. Details of the analytical and numerical calculation are reported in the supplementary information[☆].

$$\Delta T(C) = \frac{2\pi\, c(\lambda)\, V_{NP}\, n_{NP}\, I_0}{(n_{NP}\sigma_{ext})^2} \int_0^Z (\sqrt{\Xi^2+\zeta^2}-\zeta)e^{-\zeta}d\zeta \tag{1}$$

where

$$c(\lambda) = \frac{\Im(\chi_{NP})}{2\lambda k_H \sqrt{\varepsilon_H}} \left| \frac{3\varepsilon_H}{2\varepsilon_H+\varepsilon_{NP}} \right|^2, \tag{2}$$

$Z = n_{NP}\sigma_{NP}l$, $\Xi = n_{NP}\sigma_{ext}w$, $\zeta = n_{NP}\sigma_{ext}z$, n_{NP} is the NP density, σ_{ext} is the NP extinction cross section, ω is the laser beam waist on the cuvette surface, l is the cuvette height, I_0 is the laser intensity on the surface, V_{NP} is the NP volume, χ is the NP electric susceptibility, k_H is the thermal conductivity of the water, ε_H and ε_{NP} are the dielectric permittivity of the water (host medium) and of the NPs respectively.

Because of the equation 1 is not analytically solvable we calculate the integral using a numerical approach with a free software named Wxmaxima (free software released under the terms of the GNU General Public License (GPL)). For solving the integral has been used Romberg's method that evaluates the integrand at equally spaced points. The theoretical results are in good agreement with the experimental measurements, in fact, in figure 7 is reported the theoretical calculation of the temperature variation for a cylindrical sample with AuNPs density $5.85 * 10^{-5}$M illuminated with gaussian laser light with spot size 1.5mm, wavelength $\lambda = 532$ nm as a function of the laser power. The black point represents the experimental temperature variation at power light of 200 mW, the ellipse represents the error around that measurement in power and in temperature.

5. Discussion

A new generation of biocompatible and biomimetic AuNPs covered with a keratin layer has been realized and characterized. Keratin has been selected as a capping agent for AuNPs because it's a family of proteins with a unique combination of functionalities. It is a biocompatible protein that is easily sourced and characterized by many cysteine residues. The regeneration method to extract keratin, was selected to ensure the preparation of a water solution of proteins with a high amount of free thiols that will quickly and efficiently bind to the AuNPs' surface. Having all the processing done in water and mild conditions makes it easy to combine keratin with AuNPs and preserve the inherent biocompatibility of keratin. Furthermore, keratin could be further functionalized,

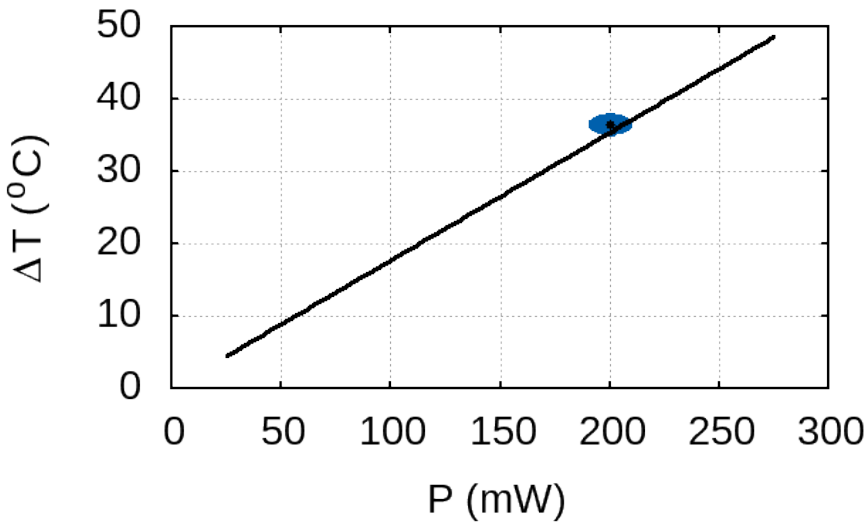

Figure 7: Temperature variation ΔT versus laser power P is predicted through equation 1 where the integral is calculated with Wxmaxima and selecting Romberg's method. A cpp program allows us to take into account different AuNPs density and different solvent. The black Point (power 200 mW; reached temperature 73 ^{o}C raised temperature 36.5 ^{o}C) represent the experimental temperature measured on the sample with AuNPs density $5.83 * 10^{-5}$ M illuminated with laser light with wavelength $\lambda = 532$ nm and power 200 mW. The ellipse represents the error along x and y direction i.e., power and temperature, respectively.

taking advantage of the dangling functional groups in the amino acid residues. As an example of functionalization, in this paper we showed tagging with a fluorescent dye. Ker-AuNPs exhibit excellent colloidal stability, high biocompatibility, and excellent photo-thermal properties. These features have been validated by performing viability assays and a PTT-based treatment by utilizing *E. coli*. Results show extraordinary biocompatibility of Ker-AuNPs since both growth and proliferation of *E. coli*, in the presence of Ker-AuNPs, at the highest concentration ($5.83 * 10^{-5}$ M), are not affected (Figure 3). Thermal experiments devoted to verifying the *E. coli* viability as a function of temperature (from 58 to 78 ^{o}C), both with and without Ker-AuNPs (Figure 4), confirm that the presence of Ker-AuNPs do not influence the typical temperature-dependent growth for the *E. coli*. Indeed, Figure 4 shows that in both cases, with Ker-AuNPs (red curve) and without (green curve), the rise in temperature leads to reduced cell viability. This trends continues up to 70 ^{o}C, where all bacteria are dead likely because of the rapid denaturation of proteins. A morphological analysis (Figure 5) performed with fluorescence and scanning electron microscopy confirms that Ker-AuNPs are well monodispersed and no signs of evident aggregation are visible. This is particularly noteworthy because it highlights the important stabilization effect provided by the keratin layer on the AuNPs surface and confirms the results shown in [20] for a different system.. The keratin functionalization enables the retention of structural (morphological, size dispersion and no aggregation) and functional (optical properties and photothermal conversion) properties even in a physiological environment rich in biomolecules and cells products. PTT-assisted viability experiments (Figure 1), performed by setting the starting temperature at 37 ^{o}C, thus mimicking the normal human body temperature condition, evidence the capability of Ker-AuNPs to generate a temperature increase of about 36 ^{o}C reaching 73 ^{o}C, thus producing a reduction in the cells viability of about 3 order of magnitudes (Figure 6, orange column). The comparison between the thermoblock experiment and the laser experiment evidences differences in the bacteria viabilitity at the same reported temperature to ascribe to the different temperature distribution inside

the sample: homogeneous in the thermoblock and localized in a point with the laser. Conversely, photo-thermal control experiments, performed in the same experimental conditions but in the absence of Ker-AuNPs (Figure 6, light blue column), evidence a negligible change (less than 1 order of magnitude) in the cells viability, thus confirming the extraordinary capability of Ker-AuNPs to convert light into thermal heating efficiently. An *ad hoc* theoretical model predicts and confirms that the measured, highest temperature (70 ^{o}C) achieved in the presence of Ker-AuNPs upon laser illumination is consistent with the utilized experimental conditions. Modeling was performed on a theoretical sample closest to the experimental condition: NPs density $5.83 * 10^{-5}$ M, laser power of about 200 mW, laser wavelength of 532 nm and beam diameter of 3 mm. Temperature was calculated at the thermal equilibrium condition (no time taken into account) because in the experiments we observe that the thermal equilibrium is reached.

Conclusions. We have reported on the synthesis, characterization, and application of a new generation of gold nanoparticles capped with keratin (Ker-AuNPs). Ker-AuNPs have been characterized in terms of morphological, spectral, and thermo-optical properties. The excellent biocompatibility of Ker-AuNPs has been tested by performing viability assay experiments of a strain of *E. coli* in the presence of a very high concentration of Ker-AuNPs (C=$5.83 * 10^{-5}$ M which is six order of magnitudes higher to the results reported in similar experiments realized with CTAB capped AuNPs [10], thus representing an important requirement for biomedical applications.). Photo-thermal experiments have confirmed the exceptional capability of Ker-AuNPs to produce a suitable temperature increase (36 ^{o}C), thus reducing the *E. coli* viability of about 3 order of magnitudes. On-going efforts are devoted to producing a new generation of Ker-AuNPs with different shapes (e.g., rods) to maximize photo-thermal efficiency while working in the water windows transparency. As such, gold nanorods (GNRs) possess very high photo-thermal efficiency (1) with superior optical ad thermo-optical properties to respect spherical AuNPs. Moreover, GNRs are

characterized by two plasmon bands (transversal and longitudinal), and one of them (longitudinal) falls in the so-called water window, where the tissue absorption is negligible. For these reasons, GNRs or other exotic AuNPs such as gold bipyramids must be considered for medical applications. However, the aim of this study was to validate the synthesis and applicability of a new generation of AuNPs made of gold and surrounded by keratin. This validation turned out to be much easier to perform with less exotic geometries such as a spherical one. Furthermore, spherical AuNPs are more easily to model, thus allowing us to obtain excellent theoretical predictions in good agreement with experimental measurements that would have been more difficult to perform with GNRs. A possible area of application might be the treatment of antibiotic-resistent bacteria (e.g. TBC). To this regard, new experiments will be performed by modifying the ker-AuNPs surface with functional groups that bind specifically to bacterial cell wall components for both in vitro and in-vivo experiments. A mouse model implanted with relevant infections (e.g., external infections implanted and localized to the peritoneal cavity of the mouse) will be studied and deeply characterized. The reported experimental results are intended to report on a new tool and a new strategy for the prevention and treatment of infections. They will allow the realization of a breakthrough drug-free novel therapeutic intervention against pathogenic diseases, with the remarkable advantage to prevent the development of antibiotic resistance in bacteria-associated infections.

Acknowledgements

The research leading to the reported results has received funding from: Air Force Office of Scientific Research (AFOSR), Air Force Research Laboratory (AFRL) and U.S. Air Force grant n^o FA9550-18-1-0038 (P. I. L. De Sio, EOARD 2017-2020) and the Materials and Manufacturing; Sapienza University of Rome, under grant n^o RM11816431206A2C (Progetto di Ateneo 2018, PI L. De Sio); POR FESR Regione Lazio Progetti Strategici NANO-TAFT, under grant n^o A0320-2019-28166; Fondazione Cariplo, grant n^o 2018-1005.

References

[1] R. Bardhan, S. Lal, A. Joshi, N. J. Halas, Theranostic nanoshells: from probe design to imaging and treatment of cancer, Accounts of chemical research 44 (10) (2011) 936–946.

[2] J. C. Castillo-Martínez, G. A. Martínez-Castañón, F. Martínez-Gutierrez, N. V. Zavala-Alonso, N. Patiño-Marín, N. Niño-Martinez, V. Zaragoza-Magaña, C. Cabral-Romero, Antibacterial and antibiofilm activities of the photothermal therapy using gold nanorods against seven different bacterial strains, Journal of Nanomaterials 2015.

[3] F. Pierini, P. Nakielski, O. Urbanek, S. Pawłowska, M. Lanzi, L. De Sio, T. A. Kowalewski, Polymer-based nanomaterials for photothermal therapy: from light-responsive to multifunctional nanoplatforms for synergistically combined technologies, Biomacromolecules 19 (11) (2018) 4147–4167.

[4] B. De Angelis, N. Depalo, F. Petronella, C. Quintarelli, M. L. Curri, R. Pani, A. Calogero, F. Locatelli, L. De Sio, Stimuli-responsive nanoparticle-assisted immunotherapy: a new weapon against solid tumours, Journal of Materials Chemistry B 8 (9) (2020) 1823–1840.

[5] L. M. Liz-Marzán, Nanometals: formation and color, feb, 2004.

[6] L. De Sio, T. Placido, R. Comparelli, M. L. Curri, M. Striccoli, N. Tabiryan, T. J. Bunning, Next-generation thermo-plasmonic technologies and plasmonic nanoparticles in optoelectronics, Progress in Quantum Electronics 41 (2015) 23–70.

[7] L. Pezzi, A. Pane, F. Annesi, M. A. Losso, A. Guglielmelli, C. Umeton, L. De Sio, Antimicrobial effects of chemically functionalized and/or photoheated nanoparticles, Materials 12 (7) (2019) 1078.

[8] J. Kimling, M. Maier, B. Okenve, V. Kotaidis, H. Ballot, A. Plech, Turkevich method for gold nanoparticle synthesis revisited, The Journal of Physical Chemistry B 110 (32) (2006) 15700–15707.

[9] B. Isomaa, J. Reuter, B. Djupsund, The subacute and chronic toxicity of cetyltrimethylammonium bromide (ctab), a cationic surfactant, in the rat, Archives of toxicology 35 (2) (1976) 91–96.

[10] F. Annesi, A. Pane, M. A. Losso, A. Guglielmelli, F. Lucente, F. Petronella, T. Placido, R. Comparelli, M. G. Guzzo, M. L. Curri, et al., Thermoplasmonic killing of *Escherichia coli* tg1 bacteria, Materials 12 (9) (2019) 1530.

[11] J. Zhang, L. Mou, X. Jiang, Surface chemistry of gold nanoparticles for health-related applications, Chemical Science 11 (4) (2020) 923–936.

[12] J. G. Rouse, M. E. Van Dyke, A review of keratin-based biomaterials for biomedical applications, Materials 3 (2) (2010) 999–1014.

[13] P. Hill, H. Brantley, M. Van Dyke, Some properties of keratin biomaterials: kerateines, Biomaterials 31 (4) (2010) 585–593.

[14] G. Suarato, M. Contardi, G. Perotto, H.-G. JoseA, F. Fiorentini, L. Ceseracciu, C. Pignatelli, D. Debellis, R. Bertorelli, A. Athanassiou, From fabric to tissue: Recovered wool keratin/polyvinylpyrrolidone biocomposite fibers as artificial scaffold platform, Materials Science and Engineering: C (2020) 111151.

[15] P. Cataldi, O. Condurache, D. Spirito, R. Krahne, I. S. Bayer, A. Athanassiou, G. Perotto, Keratin-graphene nanocomposite: Transformation of waste wool in electronic devices, ACS Sustainable Chemistry & Engineering 7 (14) (2019) 12544–12551.

[16] Q. Zhang, C. Hu, K. Yan, Preparation and characterization of silver nanoparticles from the super-heated water degraded keratin solutions, Journal of nanoscience and nanotechnology 15 (9) (2015) 6790–6797.

[17] C. D. Tran, F. Prosenc, M. Franko, G. Benzi, One-pot synthesis of biocompatible silver nanoparticle composites from cellulose and keratin: charac-

terization and antimicrobial activity, ACS Applied Materials & Interfaces 8 (50) (2016) 34791–34801.

[18] C. D. Tran, F. Prosenc, M. Franko, Facile synthesis, structure, biocompatibility and antimicrobial property of gold nanoparticle composites from cellulose and keratin, Journal of colloid and interface science 510 (2018) 237–245.

[19] S. Shankar, J.-W. Rhim, Eco-friendly antimicrobial nanoparticles of keratin-metal ion complex, Materials Science and Engineering: C 105 (2019) 110068.

[20] A. Guglielmelli, P. Rosa, M. Contardi, M. Prato, G. Mangino, S. Miglietta, V. Petrozza, R. Pani, A. Calogero, A. Athanassiou, et al., Biomimetic keratin gold nanoparticle-mediated in vitro photothermal therapy on glioblastoma multiforme, Nanomedicine (0).

[21] P. Wulandari, T. Nagahiro, N. Fukada, Y. Kimura, M. Niwano, K. Tamada, Characterization of citrates on gold and silver nanoparticles, Journal of colloid and interface science 438 (2015) 244–248.

[22] G. Perotto, G. Sandri, C. Pignatelli, G. Milanesi, A. Athanassiou, Water-based synthesis of keratin micro-and nanoparticles with tunable mucoadhesive properties for drug delivery, Journal of Materials Chemistry B 7 (28) (2019) 4385–4392.

[23] H. H. Richardson, M. T. Carlson, P. J. Tandler, P. Hernandez, A. O. Govorov, Experimental and theoretical studies of light-to-heat conversion and collective heating effects in metal nanoparticle solutions, Nano letters 9 (3) (2009) 1139–1146.

[24] A. O. Govorov, H. H. Richardson, Generating heat with metal nanoparticles, Nano today 2 (1) (2007) 30–38.

[25] A. O. Govorov, W. Zhang, T. Skeini, H. Richardson, J. Lee, N. A. Kotov, Gold nanoparticle ensembles as heaters and actuators: melting and collective plasmon resonances, Nanoscale Research Letters 1 (1) (2006) 84–90.

[26] L. Pezzi, L. De Sio, A. Veltri, T. Placido, G. Palermo, R. Comparelli, M. L. Curri, A. Agostiano, N. Tabiryan, C. Umeton, Photo-thermal effects in gold nanoparticles dispersed in thermotropic nematic liquid crystals, Physical Chemistry Chemical Physics 17 (31) (2015) 20281–20287.

[27] L. Pezzi, G. Palermo, C. Umeton, Plasmonics: A theoretical background, Active Plasmonic Nanomaterials (2015) 1.

[28] L. Pezzi, L. De Sio, G. Palermo, A. Veltri, T. Placido, M. L. Curri, N. Tabiryan, C. Umeton, Nematic liquid crystals used to control photothermal effects in gold nanoparticles, in: Emerging Liquid Crystal Technologies XI, Vol. 9769, International Society for Optics and Photonics, 2016, p. 97690C.

[29] L. Pezzi, G. Palermo, C. Umeton, A. D. Luca, Determination of nlc refractive index dispersion in wavelength and temperature for plasmonic applications, Molecular Crystals and Liquid Crystals 649 (1) (2017) 31–37. doi:10.1080/15421406.2017.1303906.

[30] L. Pezzi, L. De Sio, T. Placido, R. Comparelli, C. Umeton, Photo-induced temperature variations in plasmonic nanoparticles trapped in thermosensitive liquid crystals, Nanoscience and Nanotechnology Letters.

[31] X. Huang, P. K. Jain, I. H. El-Sayed, M. A. El-Sayed, Plasmonic photothermal therapy (pptt) using gold nanoparticles, Lasers in medical science 23 (3) (2008) 217–228.

[32] P. K. Jain, I. H. El-Sayed, M. A. El-Sayed, Au nanoparticles target cancer, nano today 2 (1) (2007) 18–29.

[33] F. X. Gu, R. Karnik, A. Z. Wang, F. Alexis, E. Levy-Nissenbaum, S. Hong, R. S. Langer, O. C. Farokhzad, Targeted nanoparticles for cancer therapy, Nano today 2 (3) (2007) 14–21.

[34] S. Lal, S. E. Clare, N. J. Halas, Nanoshell-enabled photothermal cancer therapy: impending clinical impact, Accounts of chemical research 41 (12) (2008) 1842–1851.

[35] P. Cherukuri, E. S. Glazer, S. A. Curley, Targeted hyperthermia using metal nanoparticles, Advanced drug delivery reviews 62 (3) (2010) 339–345.

[36] A. Vogel, J. Noack, G. Hüttman, G. Paltauf, Mechanisms of femtosecond laser nanosurgery of cells and tissues, Applied Physics B 81 (8) (2005) 1015–1047.

[37] A. Vogel, V. Venugopalan, Mechanisms of pulsed laser ablation of biological tissues, Chemical reviews 103 (2) (2003) 577–644.

[38] G. Han, P. Ghosh, M. De, V. M. Rotello, Drug and gene delivery using gold nanoparticles, Nanobiotechnology 3 (1) (2007) 40–45.

[39] P. Ghosh, G. Han, M. De, C. K. Kim, V. M. Rotello, Gold nanoparticles in delivery applications, Advanced drug delivery reviews 60 (11) (2008) 1307–1315.

[40] B. P. Timko, T. Dvir, D. S. Kohane, Remotely triggerable drug delivery systems, Advanced Materials 22 (44) (2010) 4925–4943.

[41] D. Boyer, P. Tamarat, A. Maali, B. Lounis, M. Orrit, Photothermal imaging of nanometer-sized metal particles among scatterers, Science 297 (5584) (2002) 1160–1163.

[42] L. Cao, D. N. Barsic, A. R. Guichard, M. L. Brongersma, Plasmon-assisted local temperature control to pattern individual semiconductor nanowires and carbon nanotubes, Nano letters 7 (11) (2007) 3523–3527.

[43] C. N. Baroud, J.-P. Delville, F. Gallaire, R. Wunenburger, Thermocapillary valve for droplet production and sorting, Physical Review E 75 (4) (2007) 046302.

[44] T. Placido, E. Fanizza, P. Cosma, M. Striccoli, M. L. Curri, R. Comparelli, A. Agostiano, Electroactive layer-by-layer plasmonic architectures based on au nanorods, Langmuir 30 (10) (2014) 2608–2618.

[45] I. Ros, T. Placido, V. Amendola, C. Marinzi, N. Manfredi, R. Comparelli, M. Striccoli, A. Agostiano, A. Abbotto, D. Pedron, et al., Sers properties of gold nanorods at resonance with molecular, transverse, and longitudinal plasmon excitations, Plasmonics 9 (3) (2014) 581–593.

[46] L. Pezzi, G. Palermo, A. Veltri, U. Cataldi, T. Bürgi, T. Ritacco, M. Giocondo, C. Umeton, A. De Luca, Photo-thermal study of a layer of randomly distributed gold nanoparticles: from nano-localization to macro-scale effects, Journal of Physics D: Applied Physics 50 (43) (2017) 435302.

[47] A. Veltri, L. Pezzi, A. De Luca, C. Umeton, Different reorientational regimes in a liquid crystalline medium undergoing multiple irradiation, Optics express 15 (4) (2007) 1663–1671.

[48] G. Palermo, D. Pagnotto, L. Ricciardi, L. Pezzi, M. La Deda, A. De Luca, Thermoplasmonic effects in gain-assisted nanoparticle solutions, The Journal of Physical Chemistry C 121 (43) (2017) 24185–24191.

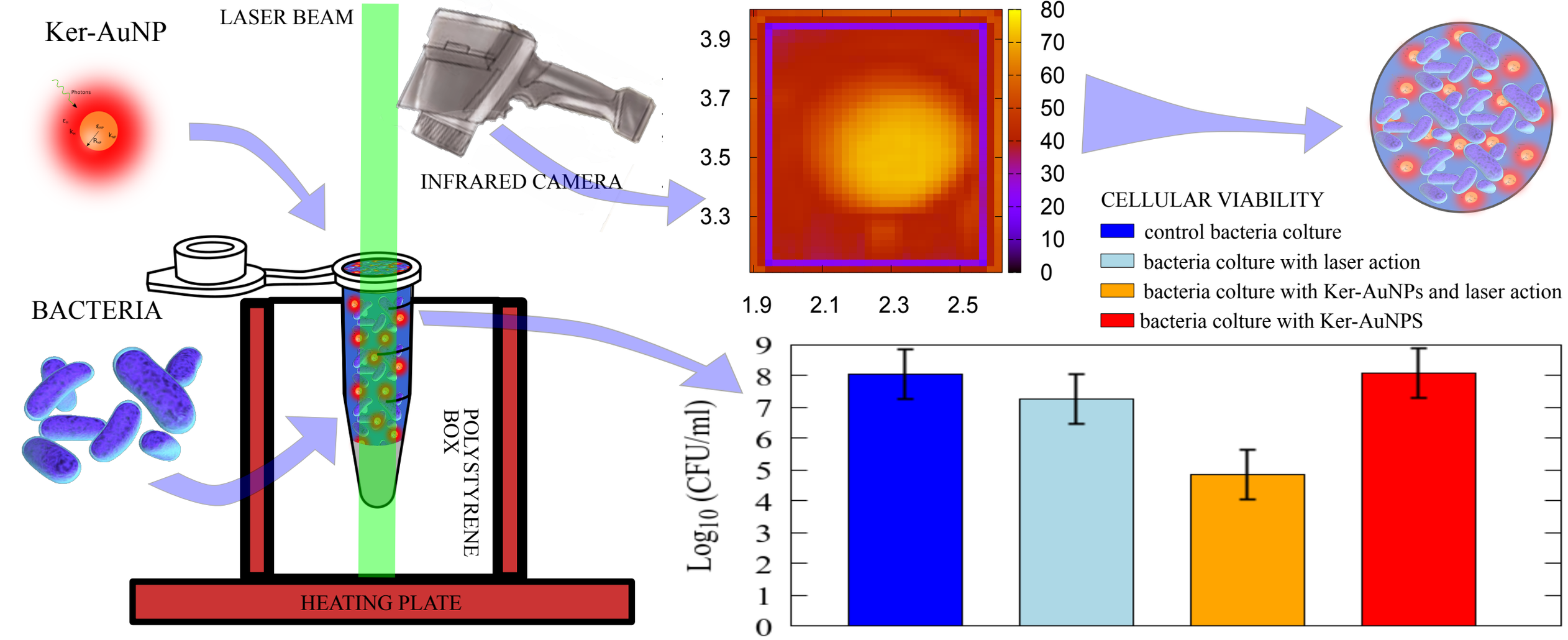
Ker-AuNP
LASER BEAM
INFRARED CAMERA
BACTERIA
POLYSTYRENE BOX
HEATING PLATE
3.9
3.7
3.5
3.3
1.9
2.1
2.3
2.5
80
70
60
50
40
30
20
10
0
CELLULAR VIABILITY
control bacteria colture
bacteria colture with laser action
bacteria colture with Ker-AuNPs and laser action
bacteria colture with Ker-AuNPS
Log10 (CFU/ml)
9
8
7
6
5
4
3
2
1
0